PHOTONICS Research

# Distributed polymer optical fiber sensors: a review and outlook

Yosuke Mizuno,[1,*] Antreas Theodosiou,[2] Kyriacos Kalli,[2] Sascha Liehr,[3] Heeyoung Lee,[4] and Kentaro Nakamura[5]

[1]Faculty of Engineering, Yokohama National University, Yokohama 240-8501, Japan
[2]Photonics and Optical Sensors Research Laboratory, Cyprus University of Technology, Limassol 3036, Cyprus
[3]DiGOS Potsdam GmbH, Telegrafenberg, Potsdam 14473, Germany
[4]College of Engineering, Shibaura Institute of Technology, Tokyo 135-8548, Japan
[5]Institute of Innovative Research, Tokyo Institute of Technology, Yokohama 226-8503, Japan
*Corresponding author: mizuno-yosuke-rg@ynu.ac.jp

Received 2 July 2021; revised 12 July 2021; accepted 12 July 2021; posted 12 July 2021 (Doc. ID 435143); published 19 August 2021

**Aging degradation and seismic damage of civil infrastructures have become a serious issue for society, and one promising technology for monitoring their conditions is optical fiber sensing. Glass optical fibers have been predominantly used for the past several decades to develop fiber sensors, but currently polymer or plastic optical fibers (POFs) have also been used extensively to develop advanced fiber sensors because of their unique features, such as high flexibility, large breakage strain, and impact resistance. This review focuses on recently developed distributed and quasi-distributed POF-based sensing techniques based on Rayleigh scattering, Brillouin scattering, and fiber Bragg gratings.** 

https://doi.org/10.1364/PRJ.435143

## 1. INTRODUCTION

Since their first proposal over half a century ago, optical fiber sensors have been continuously and extensively studied for structural health monitoring [1–5]. They have unique advantages, such as light weight, compactness, flexibility, immunity to electromagnetic interference, and the ability to provide multiplexed or distributed sensing. In multiplexed sensing, numerous discrete sensors designed to operate as point sensors are arranged in a network configuration, illuminated with a common source and with signals recovered using a shared detector. The individual sensor outputs are multiplexed onto the fiber sensing system using time-division multiplexing (TDM), wavelength-division multiplexing (WDM), spatial-division multiplexing (SDM), or combinations thereof. The inherent distributed sensing nature of optical fiber sensors enables unique configurations, for which there are no counterparts with conventional electrical sensors. Here, we focus on distributed and quasi-distributed optical fiber sensing technology.

To date, using silica glass optical fibers, a variety of distributed and quasi-distributed sensing techniques have been developed on the basis of Rayleigh scattering [6–15], Brillouin scattering [16–25], Raman scattering [26–30], and fiber gratings [31–35]. Several spatially resolved sensing techniques have been implemented, including optical time-, frequency-, and correlation-domain techniques and their combinations. Their performance parameters, such as spatial resolution, measurement range, and sampling (or repetition) rate, have been greatly improved. For instance, spatial resolution has been improved from meter to centimeter and then to (sub-)millimeter [12,13,22,23]. Simultaneous measurements of multiple physical parameters have also been achieved through numerous configurations [24,25,30,34,35]. However, these drastically enhanced performances have been mainly demonstrated using silica glass optical fibers, which are fragile and often break at relatively small strains of $<2\%-3\%$.

To overcome this fundamental issue of silica optical fibers and to add some new functionalities to existing sensors, a growing interest has been turned toward developing optical fiber sensors using polymer or plastic optical fibers (POFs) [36–45]. POFs have a number of significant merits for sensing applications, such as high flexibility in bending, large breakage strain, and high impact resistance. In addition, from the material viewpoint, although their sensing principles are often similar to those developed for conventional silica fiber sensors, POF sensors can exhibit unique properties, including extremely large (or small) sensitivities, strain and thermal memory effects [40,41], and elastic-to-plastic-transition-based phenomena.

Various types of POFs have been developed, and several types of multimode POFs are commercially available (the provision of single-mode POFs including microstructured ones is limited). Most of them have large core diameters ranging from 50 μm to 1 mm. The cores are composed of polymer materials, such as polymethylmethacrylate (PMMA), polycarbonate (PC)

[42,43], polystyrene (PS) [44], and cyclic transparent optical polymer (CYTOP; perfluorinated polymer) [45]. PMMA-, PC-, and PS-based POFs (typically, step-index fibers) have lower optical propagation loss (e.g., ~150 dB/km) at visible wavelength, but almost no light can pass through them at telecom wavelength; while CYTOP-based POFs (typically, graded-index fibers; we refer to them as perfluorinated graded-index [PFGI] POFs hereafter) still have lower propagation loss (e.g., ~50 dB/km) even at telecom wavelengths. Note that the temperature range of POFs is typically limited to a maximum of approximately 80°C–100°C, governed by their glass transition temperature.

Ten years ago, most of the POF sensors were composed of PMMA-POFs because of their wider availability and relative cost efficiency [46–55]. PMMA-POFs are still the main POFs used for developing sensors [56–59], but PFGI-POFs have also been extensively used to develop unique sensors, partly because some advanced sensing techniques developed for silica glass fiber sensors at telecom wavelengths are applicable to these fibers given their lower optical loss at these wavelengths. Although a wide variety of POF-based non-distributed sensing techniques have been reported [60–71], they are out of the scope of this paper.

Thus, in this paper, we review the recent advances in POF-based distributed and quasi-distributed sensing techniques. In Section 2, first, distributed and quasi-distributed strain, humidity, and temperature sensors based on Rayleigh scattering are described. Then, the unique properties of Brillouin scattering in POFs and its applications to distributed strain and temperature sensing are reviewed. In Section 3, quasi-distributed sensors based on fiber Bragg gratings (FBGs) are described. Finally, in Section 4, we provide concluding remarks, including some discussions on the challenges and future perspectives of POF-based sensing technology.

## 2. DISTRIBUTED SENSING TECHNIQUES

### A. Rayleigh-Based Techniques

This section introduces and summarizes POF-specific backscatter effects, Rayleigh backscatter measurement principles, and their sensing applications. Rayleigh-based sensing generally requires analysis of backscatter power or changes in backscatter power along the fiber using time- or frequency-domain reflectometry.

The multimode nature and strong mode coupling of PMMA-POFs and PFGI-POFs generally prevent the use of interferometric sensing technologies for extended distance ranges. It means that high-resolution coherent detection principles are not suitable, and therefore predominantly incoherent sensing techniques are used. The most widely used incoherent approach for backscatter analysis of PMMA-POFs and PFGI-POFs is optical time-domain reflectometry (OTDR) [72]. In particular, the photon-counting OTDR ($\nu$-OTDR) [73] is widely used for static measurement due to its high sensitivity and spatial resolution. The later development of the incoherent optical frequency-domain reflectometry (I-OFDR) for PFGI-POFs improved the spatial resolution, repetition rate, and signal stability considerably [74–76] and enabled more precise and faster measurements.

Using these distributed measurement approaches, a wide range of POF-specific effects have been studied. The extraordinary mechanical properties of POFs, the large-strain range in particular, are advantageous for Rayleigh-based distributed sensing applications. Moreover, the intrinsic susceptibility of the Rayleigh backscatter properties (backscatter coefficient and attenuation) to external influences such as strain, temperature, and humidity enabled completely new applications for truly distributed measurement. The most important Rayleigh-based effects and measurement principles are visualized in Fig. 1.

The concept of fully distributed measurement based on intrinsic effects is depicted in Figs. 1(a)–1(c). Integral fiber length change measurement $\Delta l$ is indicated in Fig. 1(a). The concept of quasi-distributed sensing based on local attenuation or backscatter increase involving a certain kind of transducing mechanism or sensitized regions along the fiber is depicted in Fig. 1(b). Distributed length change measurement in

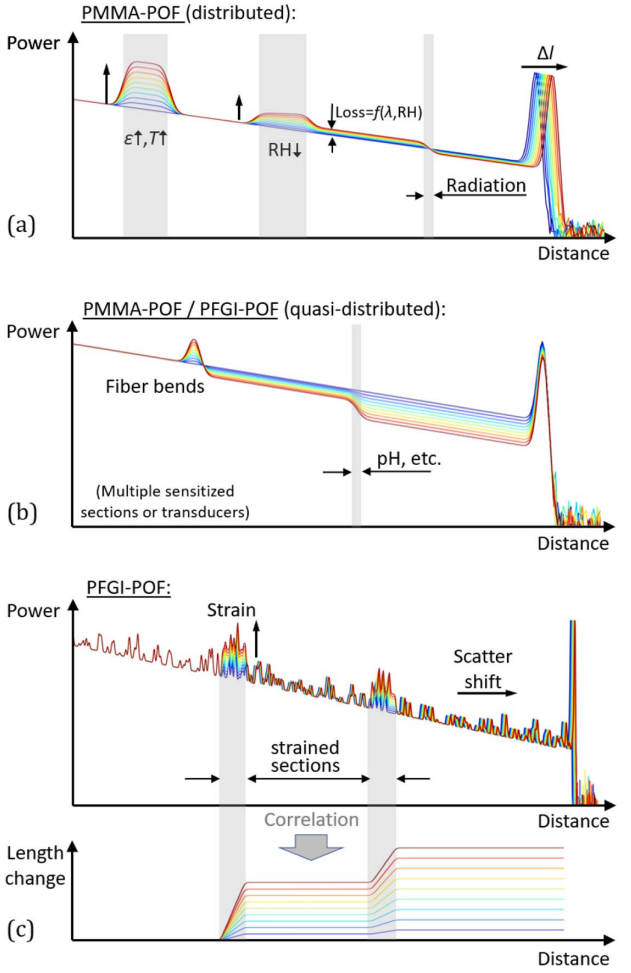


**Fig. 1.** Schematic examples for Rayleigh-based techniques. (a) Distributed Rayleigh backscatter analysis for the measurement of strain changes $\varepsilon$, temperature $T$, radiation, and RH. Length change measurement due to Fresnel reflection shift is indicated. (b) Examples for quasi-distributed sensing based on sensitized fiber sections or transducing elements. (c) Example for distributed strain sensing in PFGI-POFs and the evaluation of length change distribution from backscatter shift analysis.

**Table 1. Summary of Measurable Effects, Measurands, and Respective References for Rayleigh Backscatter-Based Sensing in POFs**

| Effects | Measurands | References |
|---|---|---|
| Distributed backscatter coefficient dependence | Strain $\varepsilon$ | [40,74–87] |
| | Humidity RH | [88,89] |
| | Temperature $T$ | [79,90] |
| Distributed attenuation | Humidity RH | [76,88,89] |
| | Radiation | [91] |
| | Cracks/deformation | [77,85,92] |
| Quasi-distributed backscatter or loss (transducer or sensitized fiber section) | Fiber bend (backscatter) | [93] |
| | Bend radius/orientation (backscatter) | [90] |
| | pH (attenuation) | [94] |
| | Humidity (attenuation) | [95] |
| Optical runtime change | Distributed strain/temperature | [75,77,96,97] |
| | Quasi-distributed/integral strain | [76,77,80,84,98] |

PFGI-POF is schematically shown in Fig. 1(c). All references in this section are listed in Table 1 and are grouped according to measurable effects and measurands. Details and examples are summarized in the following subsections.

*1. Distributed Backscatter and Attenuation Measurement*

The main reasons for using POFs for distributed sensing are their specific backscatter dependencies on strain, humidity, and temperature, but equally, their mechanical properties: PMMA-POFs can be strained up to 45% [77,79] and PFGI-POFs even up to 100% [75] and more [76]. This allows to extend the range of sensing applications far beyond the maximum strain range of silica optical fibers. Such high strain levels do exceed the materials' elastic limits but do not result in sudden fracture. The elastic strain limit depends on various properties and variables, mainly on the type of polymer and the mechanical properties of the cladding and jacketing materials used. Factors such as a strain rate, temperature, the use of dopants, and annealing conditions can also have a significant impact on the elastic strain limit and viscoelastic behavior of the fiber. Typical elastic strain ranges for POFs are in the order of 2%–5%.

Strain has the highest influence on the backscattered power level in PMMA-POFs in comparison to the temperature or RH dependence [77]. Strain-dependent backscatter change was first demonstrated in 2004 [40] and was later characterized in detail and used for distributed strain sensing applications [76,77,79–81], as seen in Fig. 1(a). The increase in backscattering with strain can mainly be attributed to an increase of Rayleigh scattering due to a creation of scattering centers at the microscopic level (micro-crazing) and at the molecular level (molecular breakdowns). The spectral evaluation of backscattered power increase from strained PMMA-POF exhibits a distinct $\lambda^{-4}$ dependence [86], which indicates a dominant contribution from Rayleigh scattering.

The backscatter increase is highly reproducible under laboratory conditions [79,87], but the temporal relaxation of the polymer core material leads to a decrease of the backscatter over time. This prevents exact strain measurement for unknown temporal strain history of the fiber. However, a localization and strain amplitude estimation can be performed. This is relevant to a wide range of large-strain applications. Hence, the focus of experimental research and field testing was on distributed large-strain sensing applications, where the strain range of silica fibers is exceeded. A range of laboratory and field applications involved the integration of PMMA-POFs into technical textiles [77]. Using these smart textiles, large-strain events in earthwork structures such as the deformation of a creeping slope were analyzed [84]. Smart textiles with integrated POFs were also deployed for crack detection and the structural health monitoring of masonry buildings [85]. OTDR backscatter analysis was similarly used for the detection of deformation of wooden structures [82] and for distributed crack detection and shear deformation measurement [92].

The attenuation of PMMA-POFs at common wavelengths of 500 and 650 nm is about 90 and 150 dB/km, respectively [88]. The distance range is in the order of 100–200 m using $\nu$-OTDR. The spatial resolution deteriorates with increasing distance due to the strong modal dispersion in these high-numerical-aperture step-index fibers. A deconvolution approach could, however, mitigate the decay of spatial resolution with increasing fiber length and reconstruct strain profiles [86].

Compared to PMMA-POFs, PFGI-POFs exhibit a significantly weaker, not linear backscatter increase with strain [75,76] and a temporal relaxation of the backscatter level [76]. Direct strain estimation from local backscatter increase is therefore less suitable with this fiber type. PFGI-POFs, however, exhibit important advantages for distributed strain sensing applications. They feature lower attenuation extending the distance range to more than 500 m [97], and they allow for continuously high spatial resolution due to their gradient-index structure and negligible modal dispersion. Strained fiber sections can be located with centimeter spatial resolution using the I-OFDR technique [75]. The location of cracks in steel specimens was detected using OTDR [83]. Distributed length change measurement in PFGI-POFs is described in Section 2.A.3.

Relative humidity (RH) has a measurable influence on the backscatter level of PMMA-POFs. As shown in Fig. 1(a), the backscatter coefficient increases by 0.083 dB per 10% decrease in RH [88]. The origin of the reduced Rayleigh scattering with increasing water content in the fiber could be attributed to a reduced inhomogeneity in the core due to reduction of refractive index differences between the polymer network and existing micro-cavities as well as within the polymer structure itself due to water uptake and filling of gaseous voids by water

molecules. An additional contribution may be due to humidity-induced swelling of the polymer, which causes a mechanically forced closing of cavities and micro-crazes, as a result of which the material inhomogeneity (and thus the Rayleigh scattering) is reduced [88].

The effect is reproducible and was demonstrated for distributed humidity sensing. The backscatter measurement was conducted at two different wavelengths: at $\lambda = 650$ nm, where $OH^-$ absorption results in an additional attenuation [Fig. 1(a)], and at $\lambda = 500$ nm, where no absorption loss occurs. The dual-wavelength analysis of backscatter dependence and attenuation dependence made it possible to distinguish RH influence from strain or temperature impact and enabled unambiguous measurement of RH. PFGI-POFs exhibit a significantly weaker backscatter dependence on RH, but a measurable dependence on attenuation and the measured length change was characterized [76]. It has been indicated that a spectral evaluation of temperature-dependent and RH-dependent absorption loss could be spatially resolved if a bi-spectral backscatter analysis is carried out at wavelengths with different absorption properties [76].

Temperature exhibits a measurable dependence on the backscatter coefficient of PMMA-POFs. The dependence is approximately linear at 0.01 dB/K and was used for distributed measurement of temperature differences along the fiber [79]. An absolute measurement of temperature can only be conducted reliably if a reference with stable backscattering power is available. The inscription of stable scattering points as absolute power references was achieved using focused femtosecond laser pulses [90]. Changes in backscattering relative to these reference points enabled absolute temperature measurement along the fiber. However, the influence of temperature on the backscatter level of PFGI-POFs is negligible [76].

Gamma radiation causes significant radiation-induced attenuation (RIA) in PFGI-POFs [99]. It was demonstrated that PFGI-POFs can be used for high-sensitivity gamma ray dosimetry with good repeatability and down to tens of grays using distributed Rayleigh backscatter loss analysis [91]. Transmission measurement results on gamma-radiated and X-ray-radiated PMMA-POFs show a by 2–3 orders of magnitude reduced radiation-induced attenuation in comparison to PFGI-POFs [100,101]. This indicates that ionizing radiation may also be used for distributed radiation detection along this fiber type. The strong spectral dependence of radiation-induced attenuation in PFGI-POFs [91,99] and PMMA-POFs [100] indicates that distributed dosimetry with tunable sensitivity may be possible by choosing specific probe wavelengths.

### 2. Quasi-Distributed Loss-Based or Scatter Change Sensors

A range of sensor principles were demonstrated that evoke either localized optical attenuation or/and local backscatter power change by means of some mechanical transducer mechanism or sensitization of one or multiple sections of the fiber. As schematically portrayed in Fig. 1(b), quasi-distributed measurement can be conducted by evaluating relative change of Rayleigh backscatter traces.

PMMA-POF OTDR measurement was, for example, used for health condition monitoring of patients under magnetic resonance imaging [93]. Here, the fiber bend-induced backscatter increase of a textile-integrated POF was analyzed during respiratory movements. Multiple positions of a PMMA-POF were sensitized to fiber bends by inscribing off-center scattering damage into the fiber core using focused femtosecond laser pulses [90]. Bend-induced change of the optical power distribution, and therefore changed interaction with the scattering damage in the fiber, allowed for the measurement of fiber bend radii as well as the orientation of the fiber bends. Quasi-distributed pH measurement was demonstrated at a cladding-removed and treated fiber section by evaluating the backscatter loss as a function of pH of an aqueous solution [94]. It has also been shown that gamma-irradiated PFGI-POF sections exhibit increased affinity to water, leading to an increase of attenuation with increasing RH. These irradiated sections may be used as quasi-distributed point sensors for RH measurement with amplified sensitivity [95].

### 3. Optical Runtime Change Measurement

The distance of scattering or reflective events in the fiber is calculated from optical runtime of the backscattered light. Changes in length or position along the fiber can therefore be measured directly if temperature-dependent [79], humidity-dependent [88] runtime changes or modal redistribution effects can be neglected or compensated for.

A linear absolute length change dependence up to 7% was already demonstrated in 2020 [80] for a PMMA-POF using OTDR and reflection shift analysis [see Fig. 1(a)]. A gradient-index PMMA-POF was characterized in the same way up to 15% strain [77]. PMMA-POFs integrated into technical textiles were used to measure length changes in a laboratory model test. The elongation of the fibers was measured during a simulated soil subsidence using a lifting cushion [77]. The result correctly corresponded to the elongation result from the evaluation of the increase in backscattering. This evaluation approach was successfully demonstrated in field tests measuring the creep velocity of a creeping slope over an extended period of time [77,84].

PFGI-POFs can endure an even higher strain range exceeding 140% [5]. They were used for dynamic and high-resolution quasi-distributed length change measurement [98]. Using a sparse sensing approach and the I-OFDR technique, length changes between reflecting events in the fiber were measured with micrometer resolution and kilohertz repetition rates. This technique was applied to measure the quasi-distributed dynamic deformation and crack formation in a masonry building on a seismic shaking table during seismic acceleration [98].

Distributed length change measurement was demonstrated in PFGI-POFs. As indicated in Fig. 1(c), PFGI-POFs typically exhibit randomly distributed strong scattering centers that are caused by particle contamination and inhomogeneities introduced during the fiber manufacturing process. These permanent scatterers can act as distance markers along the fiber. Their location and spatial shift of these scatterers were determined using a correlation analysis of overlapping fiber sections relative to a reference backscatter trace. This approach enables the measurement of distributed length change along the fiber and was first demonstrated using $\nu$-OTDR backscatter results [77,97]. The resolution could be considerably improved using I-OFDR [74–76]. Improved spatial resolution and signal

stability compared to OTDR allowed for distributed length change measurement for potentially large-strain ranges. As indicated in Fig. 1(c), distributed length change sensing can be conducted with sub-millimeter resolution and strained sections can be localized with centimeter resolution. It was also demonstrated that focused femtosecond laser pulses can be used to inscribe scattering points into the core of PFGI-POFs for potentially improved correlation results [90]. The swept wavelength interferometry technique was used to measure strain and temperature changes in a short PFGI-POF sample [96]. Large strain and temperature resolution were achieved in the laboratory, but the strong mode coupling may be an issue for large-strain measurement over longer distance using this coherent sensing technique.

### B. Brillouin-Based Techniques

#### 1. Brillouin Scattering in POFs

Brillouin scattering in optical fibers is one of the most significant nonlinear effects and has been extensively studied for distributed strain and temperature sensing [16–25]. Brillouin scattering has been characterized not only for standard silica glass fibers but for some specialty glass fibers including tellurite fibers [102,103], $As_2Se_3$ chalcogenide fibers [104,105], bismuth-oxide fibers [103,106], photonic crystal fibers [107], rare-earth-doped fibers [108], and multi-core fibers [109,110]. In addition, Brillouin scattering in POFs has also been characterized since its first observation in 2010 [111]. Here, we summarize some unique properties of Brillouin scattering in POFs, part of which are quite different from those in glass fibers and can potentially add some new functions to the conventional application field of Brillouin scattering.

First, let us review the basics of Brillouin scattering [112]. When light propagates through an optical fiber, it interacts with acoustic phonons, generating backscattered Stokes light; this phenomenon is referred to as spontaneous Brillouin scattering. The Stokes light spectrum is called the Brillouin gain spectrum (BGS), and the frequency where the peak power is obtained in the BGS is known to be downshifted by several gigahertz from the incident light; its bandwidth is related to the phonon lifetime in the material. The amount of this frequency downshift is referred to as Brillouin frequency shift (BFS), which is dependent on the applied tensile strain and ambient temperature through a change in the refractive index and the acoustic velocity (given by the Young's modulus and the density) in an optical fiber. This is the basic operating principle of Brillouin-based strain and temperature sensors.

As introduced in Section 1, quite a few types of POFs have been produced to date [36–45]. Among them, the only POFs in which Brillouin scattering has been experimentally observed so far are PFGI-POFs [45,111]. This is because they have relatively small core diameters (leading to the high optical power density) and relatively low propagation loss at 1550 nm (at which mature optical devices cultivated for telecom uses can be used). Some efforts have been made to observe Brillouin signals in other types of POFs including PMMA-POFs; successful reports have not been provided yet.

The Brillouin signals in PFGI-POFs were first observed using a conventional self-heterodyne setup composed of silica single-mode fibers (SMFs) [111]. A semiconductor laser at 1552 nm was used, and the incident optical power to the POF was controlled using an erbium-doped fiber amplifier (EDFA). The spectrum of the beat signal between the reference light and the Stokes light was observed as a BGS using an electrical spectrum analyzer (ESA). The silica SMF and the POF were butt-coupling using standard physical-contact connectors.

When the PFGI-POF with a length of 100 m and a core diameter of 120 μm was used and the incident power was 20 dBm, the BGS was clearly observed, exhibiting the BFS of ~2.8 GHz, which is approximately 4 times lower than in silica SMFs. The acoustic velocity in the POF was calculated to be approximately 1600 m/s, which is much lower than ~5500 m/s in silica SMFs, indicating that the POFs are much softer. The full width at half maximum of the BGS in the POF was 105 MHz, which is 3–4 times broader than in silica SMFs, which means that a BFS can be generated for pulse durations of a few nanoseconds. The Brillouin gain coefficient of the POF was estimated to be $\sim 3.1 \times 10^{-11}$ m/W, which is close to that of silica SMFs [$(3–5) \times 10^{-11}$ m/W], though the actual gain coefficient of the POF may be larger considering its multimode nature. The Brillouin threshold power of this 100 m-long POF was estimated to be ~24 W, which is much higher than that of silica SMFs with the same lengths, partially because of its large core diameters. This indicates that the Brillouin signals in POFs are extremely small compared to those in silica SMFs, and that it is relatively difficult to ensure a high signal-to-noise ratio (SNR) in POF-based Brillouin sensors.

The BFS dependencies on strain and temperature in POFs have also been well characterized [113]. The strain- and temperature-dependence coefficients were found to be approximately −122 MHz/% (only for small strains of <1%) and −4.1 MHz/K (or −3.2 MHz/K, depending on POF specifications), respectively. The negative signs were both different from those in silica SMFs. The absolute values of the strain and temperature coefficients are ~5 times smaller and ~3 times larger, respectively, than those in silica SMFs. This indicates that, by simply using Brillouin scattering in POFs, high-sensitivity temperature sensing with reduced strain sensitivity can be implemented.

When larger strains are applied to POFs, the BFS dependence becomes nonmonotonic [114,115]. Figure 2(a) shows the BGS dependence on large strain of up to 60%. The BFS, which was ~2.8 GHz at zero strain, decreased with strain (<2.3%) and then increased. The peak power gradually decreased with strain (>10%), while a new peak appeared at ~3.2 GHz at

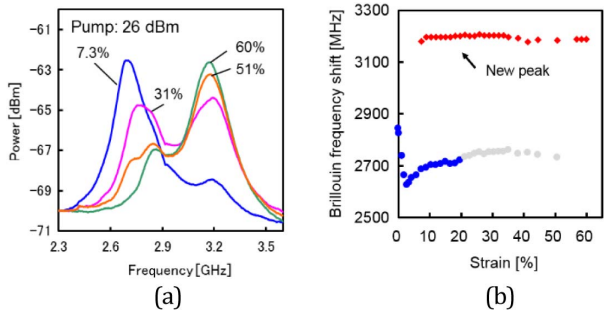


**Fig. 2.** Large-strain dependencies of (a) BGS and (b) BFS in a POF. Reproduced with permission from Ref. [115]. Copyright 2014, American Institute of Physics.

strains of >7.3%. At ~31% strain, the powers of the initial and new peaks were almost the same; at ~60% strain, the initial peak almost disappeared. The BFS dependencies of the two peaks are shown in Fig. 2(b). The initial peak showed a non-monotonic BFS dependence, while the new peak showed almost constant BFS regardless of the strain. This BFS hopping effect has been reported to be caused by strain-induced slimming of the overcladding layer composed of polycarbonate, triggered by the elastic-to-plastic transition.

After this slimming effect occurs, the strain- and temperature-dependence coefficients of the BFS of the new peak are −65.6 MHz/% (for small strains of <1%) and 4.04 MHz/K, respectively, which indicates that high-sensitivity temperature sensing with further reduced strain sensitivity is feasible [115]. When large strains of up to 30% are applied after the BFS hopping effect, the strain coefficient changed from negative to positive with a relatively small value of 16.6 MHz/%. Refer to Ref. [116] for more detailed behaviors.

Other reports on Brillouin characterization in POFs include the cross effect of strain and temperature on the BFS in POFs [117]. The BFS dependencies on humidity [118] and hydrostatic pressure [119] have also been investigated.

### 2. Strain and Temperature Sensing

To date, distributed measurement based on Brillouin scattering in POFs has been performed using three different techniques called Brillouin optical time-domain analysis (BOTDA) [17], Brillouin optical frequency-domain analysis (BOFDA) [19], and Brillouin optical correlation-domain reflectometry (BOCDR) [20]. Using BOTDA, Dong *et al.* [120] have measured the BFS distributions along POFs to investigate the evolution of mode coupling, not to perform strain and temperature sensing. In contrast, using BOFDA, Minardo *et al.* [121] have demonstrated Brillouin-based temperature sensing along a POF. They attempted to detect a 4 m-long heated section in a 20 m-long POF, but the spatial resolution was not sufficient for practical use. Here, we present BOCDR-based distributed strain and temperature sensing.

BOCDR is a distributed Brillouin sensing technique that operates on the basis of the correlation control of continuous light waves [20,122–125]. By modulating the optical frequency, what we call a correlation peak (corresponding to a sensing point) is generated and scanned along a sensing fiber. The spatial resolution and the measurement range are determined by the modulation frequency and amplitude. Refer to Ref. [125] for more detailed operating principles. The advantages of BOCDR include operation by single-end light injection, high spatial resolution, high measurement speed, random accessibility to sensing points, and cost efficiency.

Truly distributed Brillouin-based strain and temperature sensing in POFs was achieved using BOCDR in 2014 [126]. A 50 cm-long strained/heated section of a 2 m-long POF was clearly detected with a spatial resolution of 34 cm, a sampling rate of 3.3 Hz, and a higher SNR [Figs. 3(a) and 3(b)]. Then, to demonstrate a higher spatial resolution, a 10 cm-long section of a 1.3 m-long POF was heated to 40°C (high temperature sensitivity was exploited). The distributions of the BGS and the BFS measured with a spatial resolution of 7.4 cm are shown in Figs. 4(a) and 4(b), respectively. Although the SNR was not high, the heated section was clearly detected.

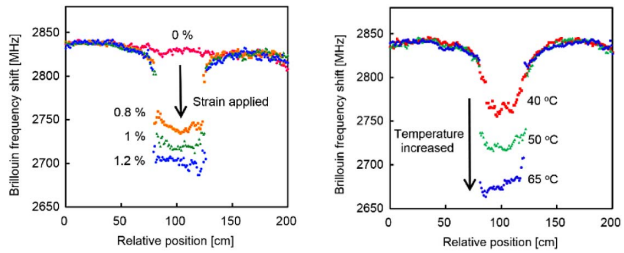


**Fig. 3.** BFS distributions measured when a 50 m-long section was (a) strained and (b) heated. Reproduced with permission from Ref. [126]. Copyright 2014, IEEE.

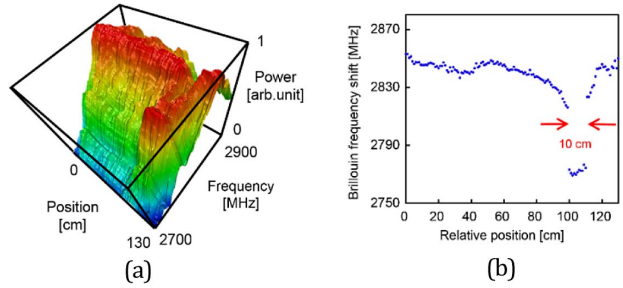


**Fig. 4.** Distributions of (a) BGS and (b) BFS, measured when a 10 cm-long section was heated. Reproduced with permission from Ref. [126]. Copyright 2014, IEEE.

A simplified configuration of BOCDR exploiting the BFS hopping effect has also been demonstrated [127]. Using the Fresnel reflection at the SMF-to-POF interface, the reference path was removed from the system. A 46 cm-long section of a 3.39 m-long POF (extended to 3.58 m) heated to 60°C was clearly detected with a spatial resolution of approximately 6 cm (largely dependent on sensing position in this configuration), as shown in Fig. 5(a). The BFS distributions measured at different temperatures [Fig. 5(b)] indicated the correct operation of this POF-based simplified BOCDR.

For faster operation, a noise-suppression technique unique to POF-based BOCDR has been developed [128]. The spectral difference between with and without reference light is acquired and the beat signal of the Brillouin-scattered light and the

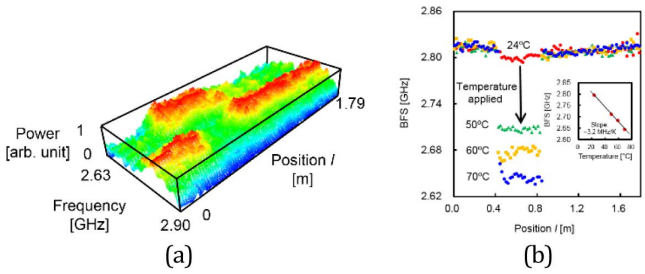


**Fig. 5.** Distributions of (a) BGS and (b) BFS, measured by simplified BOCDR when a 46 cm-long section of the POF was heated. Reproduced with permission from Ref. [127]. Copyright 2015, IEEE.

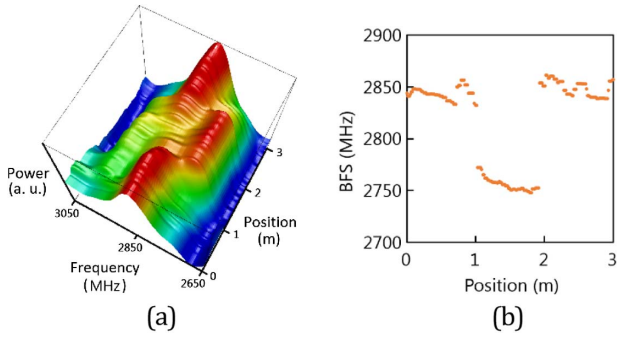


**Fig. 6.** Distributions of (a) BGS and (b) BFS, measured using a noise-suppression technique when a 1 m-long section was heated. Reproduced with permission from Ref. [128]. Copyright 2019, Optical Society of America.

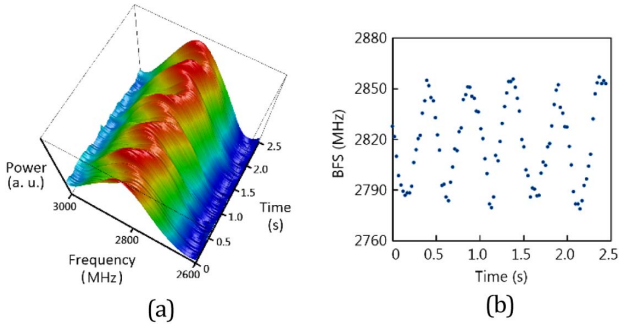


**Fig. 7.** Temporal variations of (a) BGS and (b) BFS, measured when dynamic strain was applied to a 1 m-long section. Reproduced with permission from Ref. [128]. Copyright 2019, Optical Society of America.

reference light is selectively observed. A 1.0 m-long section of a 3 m-long POF was heated to 55°C and was detected with a spatial resolution of 65 cm [Figs. 6(a) and 6(b)]. The sampling rate was 42 Hz, which was not achievable by standard BOCDR. Dynamic strain sensing was also demonstrated using this technique. A dynamic strain at 2 Hz with a magnitude of 0%–0.6% was applied to the same section of the POF. The temporal variations of the BGS and the BFS are shown in Figs. 7(a) and 7(b), respectively, which indicate dynamic strain detectability of this system. Note that the sampling rate will be increased to several hundreds of hertz by using a voltage-controlled oscillator.

Other advances on POF-based BOCDR include the clarification of the influence of the polarization scrambling [129]. Distributed strain and temperature sensing based on slope-assisted configuration has also been demonstrated at a repetition rate of 100 Hz [130].

## 3. QUASI-DISTRIBUTED FBG SENSING TECHNIQUES

### A. Multimode FBG-Based Techniques

#### 1. Characterizations

During the last few years, the potential use of practical POF sensing has resulted in great interest, and significant work has been published on quasi-distributed sensors based on CYTOP-POFs (PFGI-POFs) [131]. This was principally because of the commercial availability of such fibers, resulting in their development for short-distance communication applications [132,133], but there was a distinct lack of single-mode alternatives based on CYTOP-POFs. The sensing applications proposed covered a wide range of fields, examples of which include soft robotics, plantar pressure monitoring, health monitoring, the inspection of vibrating structures, and basic sensing applications related to the measurement of temperature and static strain.

Research on PFGI-POF-based quasi-distributed sensors has been triggered by the development of single-peak FBGs inscribed in such multimode fibers [134]. In 2016, it was shown that by controlling the spatial dimensions of the FBG in the core of the fiber, while accounting for the parabolic refractive index profile of the core, it was possible to minimize the excitation of Bragg reflections to only the first few transmission modes, even though the fiber was highly multimode [135]. As a result, more usable FBGs were fabricated in PFGI-POFs, located precisely in the fiber core, and this compared favorably to FBGs inscribed using the phase mask method [136,137] combined with pulsed ultraviolet (UV) lasers, as more clearly presented in Figs. 8(a)–8(c). Indeed, the low loss in the near infrared (IR) and the improved grating spectra made sensing arrays possible for the first time using POF [Fig. 8(d)].

As a result, PFGI-POF-FBGs were extensively characterized as sensing elements in recent years for various parameters, such as strain, RH, temperature, torsion, and pressure, while some preliminary studies were reported on their performance under

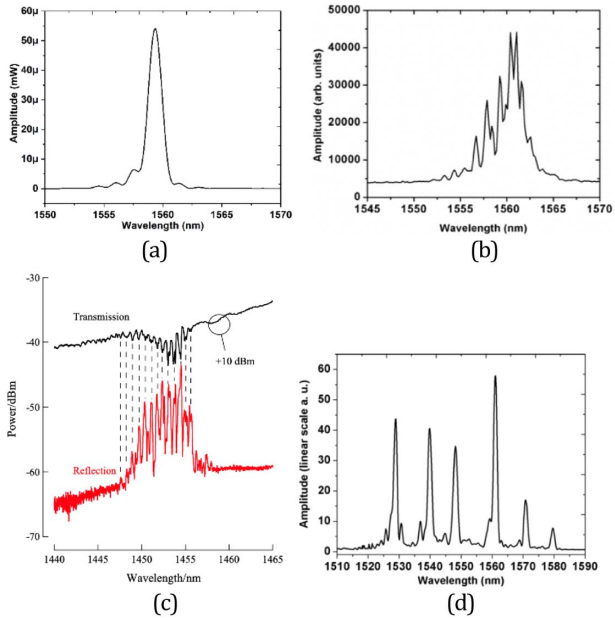


**Fig. 8.** Reflection spectra of a PFGI-POF-FBG with controlled FBG spatial dimensions using a femtosecond laser (plane-by-plane method). (a) Single-peak spectrum, (b) multiple-peak spectrum, (c) phase mask method, and (d) six-FBG array inscribed in a PFGI-POF using a femtosecond laser. Reproduced with permission from Refs. [134,136,137]. Copyright 2017, IEEE; 2018, IEEE; 2016, Elsevier.

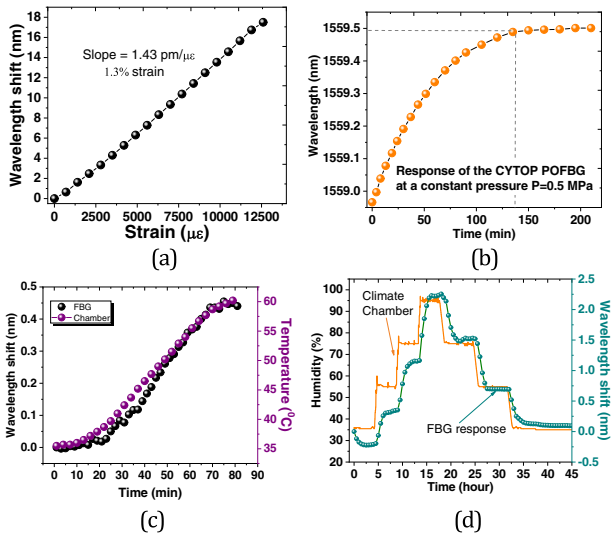


**Fig. 9.** Wavelength responses of PFGI-POF-FBGs to (a) strain, (b) pressure, (c) temperature, and (d) RH. Reproduced with permission from Refs. [131,138,139]. Copyright 2020, Elsevier; 2017, IEEE; 2017, IEEE.

ionized environments. Specifically, when the POF-FBGs inscribed in a 62.5 μm core diameter were strained, the wavelength shift of up to 18 nm with strain sensitivity ∼1.43 pm/με was obtained [Fig. 9(a)]. In terms of hydrostatic pressure sensing, the POF-FBGs showed some interesting characteristics [138]. The results show a linear wavelength shift of ∼1.3 nm/MPa in respect to hydrostatic pressure for a POF-FBG inscribed in a PFGI-POF with a 50 μm core diameter [Fig. 9(b)]. In terms of temperature sensing, reports showed that the response to the temperature varies from 5.05 pm/K up to 19.75 pm/K [140] by annealing, while other optical components such as Fabry–Perot cavities [141] showed a higher sensitivity of up to 26.4 pm/K [Fig. 9(c)]. In addition, higher-order Bragg peaks had significant temperature responses varying from 7.58 to 89.8 pm/K [142]. Negative responses can be achieved as well [143], while twisting the fiber sample indicates that control of the temperature and strain coefficients is possible.

Moreover, whereas CYTOP is not hydrophilic and cannot be used directly as RH sensors, in contrast to its PMMA counterparts [144], PFGI-POF-FBGs can perform indirect RH measurements [Fig. 9(d)] [131,139]. This is related to the polyester and polycarbonate coating surrounding the fiber, which are highly hydrophilic and swell when exposed to moisture, absorbing water, and indirectly perturbing the FBG and its

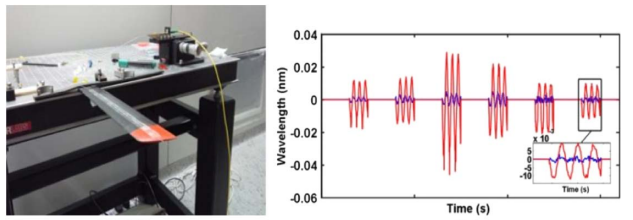


**Fig. 10.** (a) Experimental setup for monitoring the health condition of a cantilever beam. (b) Comparative vibration snapshot of the time-dependent wavelength response of a free-free metallic beam; measured using silica FBGs (blue) and PFGI-POF-FBGs (red) at the same position. Reproduced with permission from Refs. [134,139]. Copyright 2017, IEEE; 2017, IEEE.

reflection wavelength. It has been reported that a POF-FBG with hydrophilic coating with 490 μm diameter has a wavelength sensitivity to humidity of 37.6 pm/%RH [131,139].

Table 2 offers a summary of the sensitivities of POF- and silica-based FBGs to various measurands. PFGI-POF-FBGs, which share the advantages of POF sensors and offer low losses at the near-infrared region, can be regarded as promising tools for practical sensing applications. Different FBG-based components were also reported, such as chirped FBGs and Fabry–Perot cavities [141], but only as single elements.

### 2. Applications

Arrays of PFGI-POF-FBGs have been shown to have wide engineering applications, such as strain and temperature sensing [149]; mode shape capturing for structural health monitoring of different structures [134,139]; and motion monitoring of smart walkers [150], exoskeletons [151], and elastic actuators [152] with a focus on gait analysis [153–155]. Four- and six-FBG arrays were used to analyze the vibration mode shapes of a carbon helicopter blade cantilever beam [Fig. 10(a)] and a free-free metallic beam, respectively. Individual FBGs locally and instantaneously measured the beam vibration, from which the time-dependent vibration mode shape of the beams was rapidly recovered (<0.4 s). To compare and assess the POF sensor array performance, measurements using the PFGI-POF-FBG array were performed in parallel with a similar FBG array inscribed in a silica fiber. A comparison between the two arrays confirmed the potential of the POF sensor array having >8 times higher sensitivity to vibration; at the sections of the beam where the vibrating fluctuations were weak, such as the edges, the silica sensors were unable to measure the oscillations. While the silica FBGs and the POF-FBGs have similar wavelength responses to strain, the material difference greatly

**Table 2. Sensing Coefficients of FBGs Inscribed in Silica Single-Mode Fiber (SMF28), CYTOP-Based PFGI-POF, PMMA-POF, TOPAS-POF, PC-POF, and Zeonex POF[a]**

| | Silica SMF | CYTOP | PMMA | TOPAS | PC [145] | Zeonex [146] |
|---|---|---|---|---|---|---|
| $\varepsilon$ (pm/με) | 1 | 1.43 | 0.77 [147] | – | – | – |
| $T$ (pm/K) | 9.6 | 17.6 | −109 | −78 | −30.0 | −23.9 |
| RH (pm/%RH) | – | 37.6 | 34 | – | 7.31 | 6.4 |
| $P$ (nm/MPa) | 0.16 [148] | 1.5 | | | | |

[a]Note that the sensitivities for PMMA, TOPAS, PC, and Zeonex were measured at 850 nm, while those for PFGI-POF and SMF28 were at 1550 nm.

affects the transfer of strain to the sensors. Indeed, the vibration sensing data of Fig. 10(b) show this directly. As a result of the lower Young's modulus of the POF, the fiber bends more readily when vibrated and hence effectively transfers strain to the FBG. This does not occur with the glass fiber as the silica is so stiff (the Young's modulus of the glass fiber is ~20 times higher). In a similar manner, small loads of different weights were attached to different locations on a cantilever carbon helicopter blade to imitate degrees of "damage" to the beam. The location of the damage was successfully obtained using the vibration mode shapes for all of the predefined positions, and whereas the level of the damage was not ascertained, it was correlated with the time-variant fluctuation of the beam. To obtain the level of damage accurately, one requires high vibration sensitivity, which can only be offered by the POF sensors and not from their silica counterparts [Fig. 10(b)].

Progress in the use of FBG arrays in POF has resulted in interesting applications related to soft robotics and human rehabilitation. As a first application, a two-FBG array was embedded in 3D-printed wearable exoskeleton parts. The aim of this work was to show an alternative way for the development of flexible and low-cost supports for human–robot interaction force assessment. The aim of this work was the development of an assistive technology using the exoskeleton support for the rehabilitation of neurological injuries and skeletal muscles weakness using a comfortable and flexible platform. The elasticity of POF is ideal for such applications, due to the flexibility requirements of the soft robotic devices as proven by the experiment result [151]. In addition, the potential of using POF sensors instead of typical electronic sensors makes such a platform less complex and more cost effective for patients. The FBG-embedded 3D-printed supports were attached on the shank region of an exoskeleton for knee rehabilitation offering direct human–robot force assessment, as shown in Figs. 11(a) and 11(b), where the results showed the feasibility of this approach.

PFGI-POF-FBG arrays have also been used for robotic applications, such as series elastic actuators (SEAs) and in a smart walker platform [150,152]. SEAs are critical components to reduce the stiffness of robot elements and essential for the development of so-called soft robotics. They were successfully employed in wearable robotics for rehabilitation purposes with significant advantages over conventional therapies. For these components, it is essential to monitor the displacement of the spring and ensure where it is operating in the linear region. When the actuators operate linearly, the force, which is the main parameter of the therapy, is proportional to the displacement and can be measured using electronic potentiometers. However, the sensors must be precisely located in the spring, which makes the system less compact. For that reason, PFGI-POF-FBG arrays offer a promising solution to replace the electronic actuators, while offering a higher dynamic range and flexibility compared to their silica counterparts [152]. PFGI-POF-FBG arrays were inserted in an elastic actuator, and the FBGs were used to measure the torque and displacement of the actuator during movement, confirming that there are several advantages of using PFGI-POF-FBGs as elastic elements in soft robotic structures.

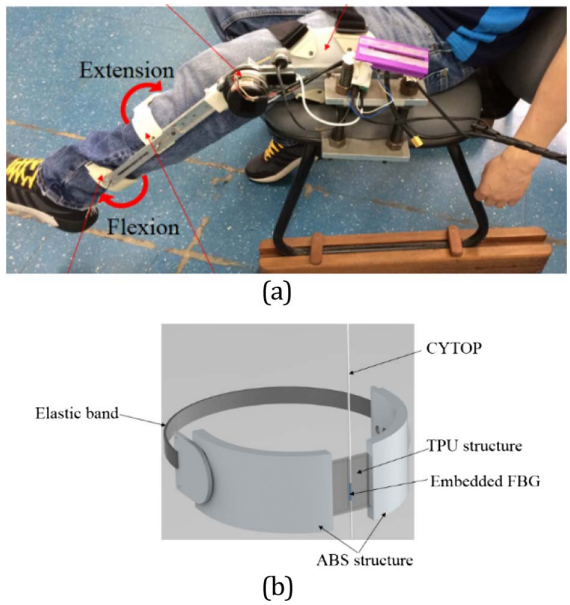


**Fig. 11.** (a) Exoskeleton with the flexible supports positioned on the shank region. (b) Schematic representation of the assembled flexible support using a PFGI-POF-FBG array, acrylonitrile butadiene styrene (ABS), and thermoplastic polyurethane (TPU). Reprinted from Ref. [151], licensed under a Creative Commons Attribution 4.0 International License.

Further applications take advantage of the load stress and durability of POFs, such as monitoring of the plantar pressure using embedded PFGI-POF-FBGs in shoe soles [153]. The sensor array proves to be useful, tracking the human gait pattern correlated with vital information regarding the spinal cord and diabetes diseases. Hence, the gait pattern recognition/analysis is an important tool for detecting the diseases and avoiding the risk of such pathologies. The gait pattern was recovered using a distributed POF-FBG array (Fig. 12). Moreover, the system had the potential to connect to a wireless network, enabling a doctor to perform real-time measurements of the patient from his office. This provides automated visual

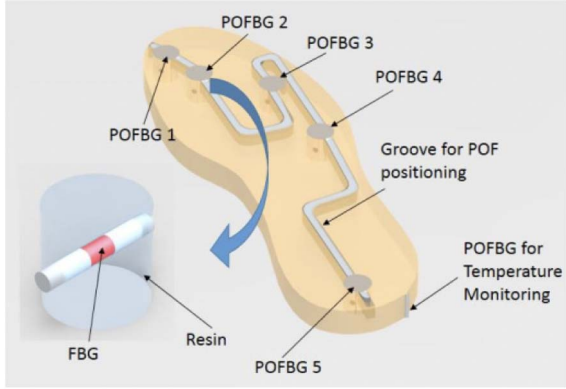


**Fig. 12.** Schematic representation of PFGI-POF-FBG array embedded in cork insole for gait pattern measurements. Reprinted from Ref. [155], licensed under a Creative Commons Attribution 4.0 International License.

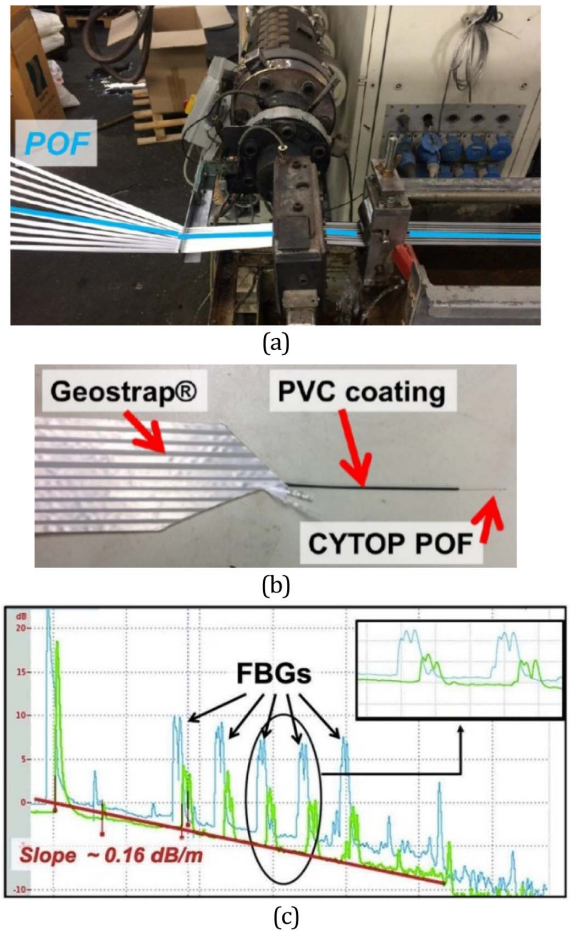


**Fig. 13.** Example of a textile bound FBG-POF sensor array. (a) The fiber embedment process, (b) the final geosynthetic strip, and (c) the OTDR trace showing the FBGs in the first 50 m of POF.

feedback using different state-of-the-art technologies (advanced optical fiber sensing technology, secured energy-efficient wireless broadband access systems, smart actuators, etc). The results with the PFGI-POF-FBGs showed an extremely good response compared to previously reported solutions using silica optical fibers [153].

An important development has been the successful embedding of the PFGI-POF, incorporating more than 30 FBGs in a 300 m fiber length, into a GeoStrap material [156]. Figure 13(a) shows the process of incorporating the POF into the GeoStrap, and the final geosynthetic strip is shown in Fig. 13(b). The fiber and the femtosecond-laser-inscribed FBGs (wavelength range: 1520–1570 nm) successfully survived a strap processing temperature of 200°C, and an OTDR trace shows the gratings recovered in the first 50 m fiber length [Fig. 13(c)]. The CYTOP fiber had a large 120 μm core diameter that was manufactured for fiber-to-the-home (FTTH) applications.

The strip was produced by crosshead extrusion coating of a polyolefin sheath over bundles of high-tenacity polyethylene terephthalate (PET) yarns. The POF containing FBGs written over its length was directly introduced in one of the extrusion channels. The mechanical performance of the strip was evaluated after production using the EN 10319 at 38.6 kN of resistance and 11.3% of deformation at break.

### B. Single-Mode FBG-Based Techniques

PMMA was the first polymer used for the fabrication of single-mode POFs (and still the most common). More specifically, they were microstructured POFs (mPOFs), which can offer endlessly single-mode operation. PMMA and TOPAS (cyclo-olefin copolymers) have been the backbone of the single-mode POF-FBG sensing technology for the last 20 years. However, the last few years, new polymers were used for the fabrication of single-mode POFs, such as polynorbornene (Zeonex) [157,158] and PC [42]. These novel POF materials improved the limited characteristics of POF-FBGs. More particularly, first-time temperature measurements up to 100°C were performed using a PC-POF while using a Zeonex POF, and the temperature limits were increased to 123°C [158]. For a particular step-index design of Zeonex POF, the inscribed FBG proved to be almost insensitive to temperature and ambient RH. Considering the high operational temperature, this offered the potential for strain measurements at high temperatures, without cross-sensitivity issues. However, even with the new POF materials, the optical characteristics of the single-mode POFs, such as the optical transmission losses, were only marginally improved compared to PMMA.

For the inscription of multiplexed single-mode POF-FBG arrays, the fabrication was primarily limited through the adoption of the phase mask inscription method with a UV-continuous-wave laser. To fabricate multiple FBG arrays using a single-phase mask, two different techniques were developed. As the first required pre-straining of the fiber, the grating period after inscription changes by a factor related to the fiber elongation applied during the inscription process. This method was well established for FBGs in silica fibers, and given the low Young's modulus of polymers, this approach has great potential for use with POFs. This was first demonstrated in POF by Yuan *et al.* [159] in 2012, where they developed a dual-FBG array in a PMMA mPOF, with a wavelength tunability for the grating of –7 nm for the application of 1% strain during inscription; beyond that point, the tuning was quickly saturated, and a significantly higher relaxation time was required after the inscription. Hence, the application of strain has affected the elastic limits of the fiber. In 2014, Rajan *et al.* [160] inscribed the longest FBG array in PMMA mPOF with five gratings, with a focus on how pre-strained levels affected the optical characteristics of the gratings. It was shown that, by maintaining the strain levels below 0.9%, the divergence between the optical characteristics of the FBGs in terms of reflectivity and bandwidth was maintained following inscription, while for higher strain levels, the grating profile was disrupted, with lower reflectivity and broader bandwidth related to creep and fiber hysteresis. The elongation limit may differ from fiber to fiber due to the different mechanical characteristics, but similar behavior is expected to be valid for fibers with similar Young's moduli.

An alternative technique to fabricate FBGs at different wavelengths using the same phase mask is through the thermal annealing method. In POFs, Johnson *et al.* [161] initially demonstrated inscription of a three-FBG array using a PMMA mPOF. To differentiate the grating wavelengths, the fiber

was heated at the temperature of 92°C, where the polymer chains are relaxed for a specific period. As the fiber is heated at the specific temperature, the fiber shrinks in length and increases in diameter. The fiber shrinkage affects the grating period, which becomes shorter, giving the potential for grating wavelength tuning up to −16 nm (a blueshift in wavelength). This phenomenon is explained as the removal of the residual internal stress of the POF that accumulates during the draw process and is introduced when the fiber is pulled under tension during the manufacturing process. In this technique, the shrinkage rate can be controlled chiefly by the duration of the annealing process and affected by the uncontrolled effects of environmental conditions, such as temperature and humidity.

The latest progress in multiple FBG array fabrication in single-mode POFs was reported in 2018 by Pospori *et al.* [147]. They developed a hybrid strain-annealing method, which has the potential to inscribe FBGs with wavelengths longer/shorter in respect to the phase mask predefined wavelength. In this work, the POF was heated with 100% humidity at a temperature between 70°C and 75°C, which is above the $\beta$-transition temperature of the material. At this temperature, the polymer releases its internal stress and molecules become mobilized, and as a result, the fiber shrinks in length. However, if sufficient axial strain is applied, the direction of the molecules can be manipulated, and when it cools down, the POF remains at the stretched position. Consequently, the grating wavelength could be tailored accordingly to wavelengths well above the original FBG position predefined by the phase mask.

Regarding the practical applications of the multiple FBG arrays in single-mode POF fibers, in addition to temperature, strain, and RH sensors, liquid level [162] and fuel monitoring in Jet A1 engines [163] have been demonstrated. A 65 cm-long five-FBG array in a PMMA-POF was fabricated using two phase masks and the annealing method. It led to 4–5 times higher sensitivity than that of a similar silica counterpart, principally related to the elasticity of the POF.

## 4. CONCLUSIONS

We have reviewed POF-based distributed and quasi-distributed sensing techniques based on Rayleigh scattering, Brillouin scattering, and FBGs. POFs exhibit a number of significant advantages for sensing applications, especially for the measurement of large strain exceeding 50%. In contrast to silica glass fibers, they are highly sensitive to various measurands, such as strain, temperature, humidity, and radiation. However, there remain several technical challenges to be tackled for a wide range of practical applications.

Responsivity to potential measurands is often associated with a limited specificity. Cross sensitivities to multiple parameters may degrade the sensor performance. This influence can be actively reduced to a certain extent by selecting special polymers (TOPAS, Zeonex, PC, etc. [42,157,158]) or by cross evaluation of secondary dependencies [88,117]. Another limiting issue, especially for large-strain sensing applications, is the viscoelastic (creep) behavior of the polymers. Temporal stress relaxation and molecular reorganization alter Rayleigh and Brillouin scattering properties over time and, if not accounted for, lead to a decrease in strain accuracy. The temperature range of standard POFs is limited to a maximum of approximately 80°C–100°C. Although high-temperature polymer fibers can extend this limitation to >120°C, the high-temperature ranges of silica glass fibers cannot be reached. Although certain measurement tasks can only be solved using POFs, the full potential of POF-based sensing has not yet been unlocked. The current unavailability of single-mode POFs with low attenuation prevents the use of more sensitive coherent measurement principles for distributed sensing. Low-loss single-mode POFs would considerably improve the performance and applicability of FBG sensors; they would also reduce the Brillouin threshold power, enhancing the SNR of distributed Brillouin sensing systems. Most optical coefficients of POFs (thermo-optic, strain-optic, BFS and its dependencies of strain, temperature, pressure, etc.) significantly differ from those of silica fibers. This would make them most suitable for multi-parameter sensing or the discrimination of measurands and cross sensitivities in a sensing configuration with parallelly deployed silica and polymer fibers.

Although these issues need to be resolved, it is an undeniable fact that POFs are attractive tools for developing distributed and quasi-distributed sensing systems with numerous advantages that silica fibers cannot provide. We anticipate that POF-based distributed sensing will be one of the most promising key technologies for achieving smart materials and structures in the future.

**Funding.** Japan Society for the Promotion of Science (17H04930, 20K22417, 21H04555); Noguchi Institute; Murata Science Foundation; Telecommunications Advancement Foundation; Yazaki Memorial Foundation for Science and Technology; Takahashi Industrial and Economic Research Foundation; European Regional Development Fund and the Republic of Cyprus through the Research and Innovation Foundation (INTEGRATED/0918/0031).

**Disclosures.** The authors declare no conflicts of interest.

**Data Availability.** Data underlying the results presented in this paper are not publicly available at this time but may be obtained from the authors upon reasonable request.

## REFERENCES

1. A. H. Hartog, *An Introduction to Distributed Optical Fibre Sensors* (CRC Press, 2017).
2. A. Motil, A. Bergman, and M. Tur, "State of the art of Brillouin fiber-optic distributed sensing," Opt. Laser Technol. **78**, 81–103 (2016).
3. B. Lee, "Review of the present status of optical fiber sensors," Opt. Fiber Technol. **9**, 57–79 (2003).
4. C. K. Y. Leung, K. T. Wan, D. Inaudi, X. Bao, W. Habel, Z. Zhou, J. Ou, M. Ghandehari, H. C. Wu, and M. Imai, "Review: optical fiber sensors for civil engineering applications," Mater. Struct. **48**, 871–906 (2015).
5. K. L. Brogan and D. R. Walt, "Optical fiber-based sensors: application to chemical biology," Curr. Opin. Chem. Biol. **9**, 494–500 (2005).
6. A. H. Hartog and D. N. Payne, "Remote measurement of temperature distribution using an optical fibre," in *European Conference on Optical Communication (ECOC)* (1982), pp. 215–220.

7. M. Froggatt and J. Moore, "High-spatial-resolution distributed strain measurement in optical fiber with Rayleigh scatter," Appl. Opt. **37**, 1735–1740 (1998).
8. S. V. Shatalin, V. N. Treschikov, and A. J. Rogers, "Interferometric optical time-domain reflectometry for distributed optical-fiber sensing," Appl. Opt. **37**, 5600–5604 (1998).
9. A. K. Sang, M. E. Froggatt, D. K. Gifford, S. T. Kreger, and B. D. Dickerson, "One centimeter spatial resolution temperature measurements in a nuclear reactor using Rayleigh scatter in optical fiber," IEEE Sens. J. **8**, 1375–1380 (2008).
10. Y. Koyamada, M. Imahama, K. Kubota, and K. Hogari, "Fiber-optic distributed strain and temperature sensing with very high measurand resolution over long range using coherent OTDR," J. Lightwave Technol. **27**, 1142–1146 (2009).
11. T. Chen, Q. Wang, R. Chen, B. Zhang, K. P. Chen, M. Maklad, and P. R. Swinehart, "Distributed hydrogen sensing using in-fiber Rayleigh scattering," Appl. Phys. Lett. **100**, 191105 (2012).
12. J. Song, W. Li, P. Lu, Y. Xu, L. Chen, and X. Bao, "Long-range high spatial resolution distributed temperature and strain sensing based on optical frequency-domain reflectometry," IEEE Photon. J. **6**, 6801408 (2014).
13. J. Pastor-Graells, H. F. Martins, A. Garcia-Ruiz, S. Martin-Lopez, and M. Gonzalez-Herraez, "Single-shot distributed temperature and strain tracking using direct detection phase sensitive OTDR with chirped pulses," Opt. Express **24**, 13121–13133 (2016).
14. A. Yan, S. Huang, S. Li, R. Chen, P. Ohodnicki, M. Buric, S. Lee, M.-J. Li, and K. P. Chen, "Distributed optical fiber sensors with ultrafast laser enhanced Rayleigh backscattering profiles for real-time monitoring of solid oxide fuel cell operations," Sci. Rep. **7**, 9369 (2017).
15. P. Lu, S. J. Mihailov, D. Coulas, H. Ding, and X. Bao, "Low loss random fiber gratings made with a fs-IR laser for distributed fiber sensing," J. Lightwave Technol. **37**, 4697–4702 (2019).
16. T. Kurashima, T. Horiguchi, H. Izumita, S. Furukawa, and Y. Koyamada, "Brillouin optical-fiber time domain reflectometry," IEICE Trans. Commun. **E76-B**, 382–390 (1993).
17. T. Horiguchi and M. Tateda, "BOTDA—nondestructive measurement of single-mode optical fiber attenuation characteristics using Brillouin interaction: theory," J. Lightwave Technol. **7**, 1170–1176 (1989).
18. A. Minardo, R. Bernini, R. Ruiz-Lombera, J. Mirapeix, J. M. Lopez-Higuera, and L. Zeni, "Proposal of Brillouin optical frequency-domain reflectometry (BOFDR)," Opt. Express **24**, 29994–30001 (2016).
19. D. Garus, K. Krebber, F. Schliep, and T. Gogolla, "Distributed sensing technique based on Brillouin optical-fiber frequency-domain analysis," Opt. Lett. **21**, 1402–1404 (1996).
20. Y. Mizuno, W. Zou, Z. He, and K. Hotate, "Proposal of Brillouin optical correlation-domain reflectometry," Opt. Express **16**, 12148–12153 (2008).
21. K. Hotate and T. Hasegawa, "Measurement of Brillouin gain spectrum distribution along an optical fiber using a correlation-based technique—proposal, experiment and simulation," IEICE Trans. Electron. **E83-C**, 405–412 (2000).
22. A. Denisov, M. A. Soto, and L. Thévenaz, "Going beyond 1000000 resolved points in a Brillouin distributed fiber sensor: theoretical analysis and experimental demonstration," Light Sci. Appl. **5**, e16074 (2016).
23. Y. H. Kim, K. Lee, and K. Y. Song, "Brillouin optical correlation domain analysis with more than 1 million effective sensing points based on differential measurement," Opt. Express **23**, 33241–33248 (2015).
24. M. Ding, Y. Mizuno, and K. Nakamura, "Discriminative strain and temperature measurement using Brillouin scattering and fluorescence in erbium-doped optical fiber," Opt. Express **22**, 24706–24712 (2014).
25. W. Zou, Z. He, and K. Hotate, "Complete discrimination of strain and temperature using Brillouin frequency shift and birefringence in a polarization-maintaining fiber," Opt. Express **17**, 1248–1255 (2009).
26. G. Bolognini and A. Hartog, "Raman-based fibre sensors: trends and applications," Opt. Fiber Technol. **19**, 678–688 (2013).
27. M. Wang, H. Wu, M. Tang, Z. Zhao, Y. Dang, C. Zhao, R. Liao, W. Chen, S. Fu, C. Yang, W. Tong, P. P. Shum, and D. Liu, "Few-mode fiber based Raman distributed temperature sensing," Opt. Express **25**, 4907–4916 (2017).
28. D. Hwang, D.-J. Yoon, I.-B. Kwon, D.-C. Seo, and Y. Chung, "Novel auto-correction method in a fiber-optic distributed-temperature sensor using reflected anti-Stokes Raman scattering," Opt. Express **18**, 9747–9754 (2010).
29. M. K. Saxena, S. D. V. S. J. Raju, R. Arya, R. B. Pachori, S. V. G. Ravindranath, S. Kher, and S. M. Oak, "Raman optical fiber distributed temperature sensor using wavelet transform based simplified signal processing of Raman backscattered signals," Opt. Laser Technol. **65**, 14–24 (2015).
30. Y.-G. Han, T. V. A. Tran, S.-H. Kim, and S. B. Lee, "Multiwavelength Raman-fiber-laser-based long-distance remote sensor for simultaneous measurement of strain and temperature," Opt. Lett. **30**, 1282–1284 (2005).
31. Y. Wang, J. Gong, D. Y. Wang, B. Dong, W. Bi, and A. Wang, "A quasi-distributed sensing network with time-division-multiplexed fiber Bragg gratings," IEEE Photon. Technol. Lett. **23**, 70–72 (2011).
32. B. A. Wilson and T. E. Blue, "Quasi-distributed temperature sensing using type-II fiber Bragg gratings in sapphire optical fiber to temperatures up to 1300°C," IEEE Sens. J. **18**, 8345–8351 (2018).
33. G. Liang, J. Jiang, K. Liu, S. Wang, T. Xu, W. Chen, Z. Ma, Z. Ding, X. Zhang, Y. Zhang, and T. Liu, "Phase demodulation method based on a dual-identical-chirped-pulse and weak fiber Bragg gratings for quasi-distributed acoustic sensing," Photon. Res. **8**, 1093–1099 (2020).
34. M. A. Davis and A. D. Kersey, "Simultaneous measurement of temperature and strain using fiber Bragg gratings and Brillouin scattering," Proc. SPIE **2838**, 114–123 (1996).
35. I. Toccafondo, M. Taki, A. Signorini, F. Zaidi, T. Nannipieri, S. Faralli, and F. D. Pasquale, "Hybrid Raman/fiber Bragg grating sensor for distributed temperature and discrete dynamic strain measurements," Opt. Lett. **37**, 4434–4436 (2012).
36. M. G. Kuzyk, *Polymer Fiber Optics: Materials, Physics, and Applications* (CRC Press, 2006).
37. O. Ziemann, J. Krauser, P. E. Zamzow, and W. Daum, *POF: Polymer Optical Fibers for Data Communication* (Springer, 2002).
38. K. Peters, "Polymer optical fiber sensors—a review," Smart Mater. Struct. **20**, 013002 (2010).
39. J. Zubia and J. Arrue, "Plastic optical fibers: an introduction to their technological processes and applications," Opt. Fiber Technol. **7**, 101–140 (2001).
40. I. R. Husdi, K. Nakamura, and S. Ueha, "Sensing characteristics of plastic optical fibres measured by optical time-domain reflectometry," Meas. Sci. Technol. **15**, 1553–1559 (2004).
41. K. Minakawa, N. Hayashi, Y. Mizuno, and K. Nakamura, "Thermal memory effect in polymer optical fibers," IEEE Photon. Technol. Lett. **27**, 1394–1397 (2015).
42. A. Fasano, G. Woyessa, P. Stajanca, C. Markos, A. Stefani, K. Nielsen, H. K. Rasmussen, K. Krebber, and O. Bang, "Fabrication and characterization of polycarbonate microstructured polymer optical fibers for high-temperature-resistant fiber Bragg grating strain sensors," Opt. Mater. Express **6**, 649–659 (2016).
43. T. Kaino, M. Fujiki, and S. Nara, "Low-loss polystyrene core-optical fibers," J. Appl. Phys. **52**, 7061–7063 (1981).
44. B. S. Rao, J. B. Puschett, and K. Matyjaszewski, "Preparation of pH sensors by covalent linkage of dye molecules to the surface of polystyrene optical fibers," J. Appl. Polym. Sci. **43**, 925–928 (1991).
45. Y. Koike and M. Asai, "The future of plastic optical fiber," NPG Asia Mater. **1**, 22–28 (2009).
46. S. Kiesel, K. Peters, T. Hassan, and M. Kowalsky, "Large deformation in-fiber polymer optical fiber sensor," IEEE Photon. Technol. Lett. **20**, 416–418 (2008).
47. Z. Xie, J. Tao, Y. Lu, K. Lin, J. Yan, P. Wang, and H. Ming, "Polymer optical fiber SERS sensor with gold nanorods," Opt. Commun. **282**, 439–442 (2009).
48. K. E. Carroll, C. Zhang, D. J. Webb, K. Kalli, A. Argyros, and M. C. J. Large, "Thermal response of Bragg gratings in PMMA microstructured optical fibers," Opt. Express **15**, 8844–8850 (2007).
49. S. Binu, K. Kochunarayanan, V. P. M. Pillai, and N. Chandrasekaran, "PMMA (polymethyl methacrylate) fiber optic probe as a noncontact

liquid level sensor," Microw. Opt. Technol. Lett. **52**, 2114–2118 (2010).
50. E. Alvarado-Méndez, R. Rojas-Laguna, J. A. Andrade-Lucio, D. Hernández-Cruz, R. A. Lessard, and J. G. Aviña-Cervantes, "Design and characterization of pH sensor based on sol–gel silica layer on plastic optical fiber," Sens. Actuators B Chem. **106**, 518–522 (2005).
51. M. Bottacini, N. Burani, M. Foroni, F. Poli, and S. Selleri, "All-plastic optical-fiber level sensor," Microw. Opt. Technol. Lett. **46**, 520–522 (2005).
52. P. G. Lye, M. Boerkamp, A. Ernest, and D. W. Lamb, "Investigating the sensitivity of PMMA optical fibres for use as an evanescent field absorption sensor in aqueous solutions," J. Phys. Conf. Ser. **15**, 262–269 (2005).
53. M. Silva-López, A. Fender, W. N. MacPherson, J. S. Barton, J. D. C. Jones, D. Zhao, H. Dobb, D. J. Webb, L. Zhang, and I. Bennion, "Strain and temperature sensitivity of a single-mode polymer optical fiber," Opt. Lett. **30**, 3129–3131 (2005).
54. H. Chibani, K. Dukenbayev, M. Mensi, S. K. Sekatskii, and G. Dietler, "Near-field scanning optical microscopy using polymethylmethacrylate optical fiber probes," Ultramicroscopy **110**, 211–215 (2010).
55. D. Gallego and H. Lamela, "High-sensitivity ultrasound interferometric single-mode polymer optical fiber sensors for biomedical applications," Opt. Lett. **34**, 1807–1809 (2009).
56. H. Lv, K. Zhang, X. Ma, W. Zhong, Y. Wang, and X. Gao, "Optimum design of the surface plasmon resonance sensor based on polymethyl methacrylate fiber," Phys. Open **6**, 100054 (2021).
57. Z. Samavati, A. Samavati, A. F. Ismail, N. Yahya, M. A. Rahman, and M. H. D. Othman, "Effect of acetone/methanol ratio as a hybrid solvent on fabrication of polymethylmethacrylate optical fiber sensor," Opt. Laser Technol. **123**, 105896 (2020).
58. C. Lyu, Z. Liu, Z. Huo, C. Ge, X. Cheng, and H.-Y. Tam, "High-sensitivity, high-spatial-resolution distributed strain sensing based on a poly(methyl methacrylate) chirped fiber Bragg grating," Photon. Res. **8**, 1134–1139 (2020).
59. S. Muthusamy, J. Charles, B. Renganathan, and A. R. Ganesan, "Ternary polypyrrole/prussian blue/$TiO_2$ nanocomposite wrapped poly-methyl methacrylate fiber optic gas sensor to detect volatile gas analytes," Optik **230**, 166289 (2021).
60. S. Cao, Y. Shao, Y. Wang, T. Wu, L. Zhang, Y. Huang, F. Zhang, C. Liao, J. He, and Y. Wang, "Highly sensitive surface plasmon resonance biosensor based on a low-index polymer optical fiber," Opt. Express **26**, 3988–3994 (2018).
61. D. Haroglu, N. Powell, and A.-F. M. Seyam, "The response of polymer optical fiber (POF) to cyclic loading for the application of a POF sensor for automotive seat occupancy sensing," J. Text. Inst. **108**, 42–48 (2017).
62. T. Kawa, G. Numata, H. Lee, N. Hayashi, Y. Mizuno, and K. Nakamura, "Temperature sensing based on multimodal interference in polymer optical fibers: room-temperature sensitivity enhancement by annealing," Jpn. J. Appl. Phys. **56**, 078002 (2017).
63. Y. Mizuno, S. Hagiwara, N. Matsutani, K. Noda, H. Lee, and K. Nakamura, "Observation of multimodal interference in millimeter-long polymer optical fibers," IEICE Electron. Express **16**, 20190135 (2019).
64. S. Shimada, H. Lee, M. Shizuka, H. Tanaka, N. Hayashi, Y. Matsumoto, Y. Tanaka, H. Nakamura, Y. Mizuno, and K. Nakamura, "Refractive index sensing using ultrasonically crushed polymer optical fibers," Appl. Phys. Express **10**, 012201 (2017).
65. Y. Mizuno, H. Lee, S. Shimada, Y. Matsumoto, Y. Tanaka, H. Nakamura, and K. Nakamura, "Pilot demonstration of refractive index sensing using polymer optical fiber crushed with slotted screwdriver," IEICE Electron. Express **14**, 20170962 (2017).
66. G. Numata, N. Hayashi, Y. Mizuno, and K. Nakamura, "Ultra-sensitive strain and temperature sensing based on modal interference in perfluorinated polymer optical fibers," IEEE Photon. J. **6**, 6802306 (2014).
67. H. Ujihara, N. Hayashi, K. Minakawa, Y. Mizuno, and K. Nakamura, "Polymer optical fiber tapering without the use of external heat source and its application to refractive index sensing," Appl. Phys. Express **8**, 072501 (2015).
68. Y. Mizuno, G. Numata, T. Kawa, H. Lee, N. Hayashi, and K. Nakamura, "Multimodal interference in perfluorinated polymer optical fibers: application to ultrasensitive strain and temperature sensing," IEICE Trans. Electron. **E101-C**, 602–610 (2018).
69. A. Leal-Junior, A. Frizera, M. J. Pontes, P. Antunes, N. Alberto, M. F. Domingues, H. Lee, R. Ishikawa, Y. Mizuno, K. Nakamura, P. André, and C. Marques, "Dynamic mechanical analysis on fused polymer optical fibers: towards sensor applications," Opt. Lett. **43**, 1754–1757 (2018).
70. A. Leal-Junior, A. Frizera, H. Lee, Y. Mizuno, K. Nakamura, T. Paixão, C. Leitão, M. F. Domingues, N. Alberto, P. Antunes, P. André, C. Marques, and M. J. Pontes, "Strain, temperature, moisture, and transverse force sensing using fused polymer optical fibers," Opt. Express **26**, 12939–12947 (2018).
71. A. Leal-Junior, A. Frizera, H. Lee, Y. Mizuno, K. Nakamura, C. Leitão, M. F. Domingues, N. Alberto, P. Antunes, P. André, C. Marques, and M. J. Pontes, "Design and characterization of a curvature sensor using fused polymer optical fibers," Opt. Lett. **43**, 2539–2542 (2018).
72. M. K. Barnoski and S. M. Jensen, "Fiber waveguides—a novel technique for investigating attenuation characteristics," Appl. Opt. **15**, 2112–2115 (1976).
73. P. Eraerds, M. Legre, J. Zhang, H. Zbinden, and N. Gisin, "Photon counting OTDR: advantages and limitations," J. Lightwave Technol. **28**, 952–964 (2010).
74. S. Liehr, N. Nöther, and K. Krebber, "Incoherent optical frequency domain reflectometry and distributed strain detection in polymer optical fibers," Meas. Sci. Technol. **21**, 017001 (2010).
75. S. Liehr, M. Wendt, and K. Krebber, "Distributed strain measurement in perfluorinated polymer optical fibres using optical frequency domain reflectometry," Meas. Sci. Technol. **21**, 094023 (2010).
76. S. Liehr, *Fibre Optic Sensing Techniques Based on Incoherent Optical Frequency Domain Reflectometry* (BAM Dissertationsreihe, 2015), p. 125.
77. S. Liehr, P. Lenke, M. Wendt, K. Krebber, M. Seeger, E. Thiele, H. Metschies, B. Gebreselassie, and J. C. Munich, "Polymer optical fiber sensors for distributed strain measurement and application in structural health monitoring," IEEE Sens. J. **9**, 1330–1338 (2009).
78. K. Nakamura, I. R. Husdi, and S. Ueha, "A distributed strain sensor with the memory effect based on the POF OTDR," Proc. SPIE **5855**, 807–810 (2005).
79. S. Liehr, P. Lenke, K. Krebber, M. Seeger, E. Thiele, H. Metschies, B. Gebreselassie, J. C. Münich, and L. Stempniewski, "Distributed strain measurement with polymer optical fibers integrated into multifunctional geotextiles," Proc. SPIE **7003**, 700302 (2008).
80. T. Gordelier, P. R. Thies, G. Rinaldi, and L. Johanning, "Investigating polymer fibre optics for condition monitoring of synthetic mooring lines," J. Mar. Sci. Eng. **8**, 103 (2020).
81. P. Lenke, S. Liehr, K. Krebber, F. Weigand, and E. Thiele, "Distributed strain measurement with polymer optical fiber integrated in technical textiles using the optical time domain reflectometry technique," in *16th International Conference on Plastic Optical Fibers* (2007), pp. 21–24.
82. T. Fukumoto, K. Nakamura, and S. Ueha, "A POF-based distributed strain sensor for detecting deformation of wooden structures," Proc. SPIE **7004**, 700469 (2008).
83. R. Suresh and K. S. C. Kuang, "Crack detection of a tensile steel specimen using plastic optical fibre sensor," Int. J. Struct. Eng. **7**, 367–377 (2016).
84. S. Liehr, P. Lenke, M. Wendt, K. Krebber, R. Gloetzl, J. Schneider-Gloetzl, L. Gabino, and L. Krywult, "Distributed polymer optical fiber sensors in geotextiles for monitoring of earthwork structures," in *4th International Conference Structural Health Monitoring of Intelligent Infrastructure (SHMII-4)* (2009).
85. S. Liehr, M. Wendt, J. C. Münich, L. Stempniewski, and H. Metschies, "Distributed polymer optical fiber sensors integrated in technical textiles for monitoring of masonry structures," in *4th International Conference Structural Health Monitoring of Intelligent Infrastructure (SHMII-4)* (2009).
86. P. Lenke, S. Liehr, and K. Krebber, "Improvements of the distributed strain sensor based on optical time domain reflectometry

measurement in polymer optical fibers," in *17th International Conference on Plastic Optical Fibers* (2008).
87. S. Dengler, N. Schmidt, M. Luber, J. Fischer, O. Ziemann, R. Engelbrecht, and H. Hangen, "Influence of temporal strain evolution on distributed strain sensing with OTDR in polymer optical fibers," in *SMSI 2020—Sensors and Instrumentation* (2020), pp. 75–76.
88. S. Liehr, M. Breithaupt, and K. Krebber, "Distributed humidity sensing in PMMA optical fibers at 500 nm and 650 nm wavelengths," Sensors **17**, 738 (2017).
89. P. Lenke, M. Wendt, S. Liehr, and K. Krebber, "Distributed humidity sensing based on Rayleigh scattering in polymer optical fibers," Proc. SPIE **7653**, 765364 (2010).
90. S. Liehr, J. Burgmeier, K. Krebber, and W. Schade, "Femtosecond laser structuring of polymer optical fibers for backscatter sensing," J. Lightwave Technol. **31**, 1418–1425 (2013).
91. P. Stajanca and K. Krebber, "Radiation-induced attenuation of perfluorinated polymer optical fibers for radiation monitoring," Sensors **17**, 1959 (2017).
92. T. Y. P. Yuen, C.-A. Tsai, T. Deb, Y.-H. Lin, J. Nyienyi, K. T. Wan, and Q. Huang, "Large structural shear deformation and failure monitoring using bend losses in polymer optical fibre," Sensors **20**, 195 (2020).
93. J. Witt, F. Narbonneau, M. Schukar, K. Krebber, J. D. Jonckheere, M. Jeanne, D. Kinet, B. Paquet, A. Depre, L. T. D'Angelo, T. Thiel, and R. Logier, "Medical textiles with embedded fiber optic sensors for monitoring of respiratory movement," IEEE Sens. J. **12**, 246–254 (2012).
94. C. Saunders and P. J. Scully, "Distributed plastic optical fibre measurement of pH using a photon counting OTDR," J. Phys. Conf. Ser. **15**, 61–66 (2005).
95. P. Stajanca, L. Mihai, D. Sporea, D. Negut, H. Sturm, M. Schukar, and K. Krebber, "Impacts of gamma irradiation on CYTOP plastic optical fibres," in *25th International Conference on Plastic Optical Fibers* (2016).
96. S. T. Kreger, A. K. Sang, D. K. Gifford, and M. E. Froggatt, "Distributed strain and temperature sensing in plastic optical fiber using Rayleigh scatter," Proc. SPIE **7316**, 73160A (2009).
97. S. Liehr, P. Lenke, M. Wendt, and K. Krebber, "Perfluorinated graded-index polymer optical fibers for distributed measurement of strain," in *17th International Conference on Plastic Optical Fibers* (2008).
98. S. Liehr and K. Krebber, "Application of quasi-distributed and dynamic length and power change measurement using optical frequency domain reflectometry," IEEE Sens. J. **12**, 237–245 (2012).
99. P. Stajanca, L. Mihai, D. Sporea, D. Neguţ, H. Sturm, M. Schukar, and K. Krebber, "Effects of gamma radiation on perfluorinated polymer optical fibers," Opt. Mater. **58**, 226–233 (2016).
100. S. O'Keeffe and E. Lewis, "Polymer optical fibre for in situ monitoring of gamma radiation processes," Int. J. Smart Sens. Intell. Syst. **2**, 490–502 (2009).
101. O. J. Olusoji, W. Kam, and S. O'Keeffe, "Radiotherapy dosimetry based on perfluorinated polymer optical fibers," Proc. SPIE **11354**, 113541W (2020).
102. Y. Mizuno, Z. He, and K. Hotate, "Distributed strain measurement using a tellurite glass fiber with Brillouin optical correlation-domain reflectometry," Opt. Commun. **283**, 2438–2441 (2010).
103. Y. Mizuno, Z. He, and K. Hotate, "Dependence of the Brillouin frequency shift on temperature in a tellurite glass fiber and a bismuth-oxide highly-nonlinear fiber," Appl. Phys. Express **2**, 112402 (2009).
104. K. S. Abedin, "Observation of strong stimulated Brillouin scattering in single-mode $As_2Se_3$ chalcogenide fiber," Opt. Express **13**, 10266–10271 (2005).
105. K. Y. Song, K. S. Abedin, K. Hotate, M. G. Herráez, and L. Thévenaz, "Highly efficient Brillouin slow and fast light using $As_2Se_3$ chalcogenide fiber," Opt. Express **14**, 5860–5865 (2006).
106. J. Lee, T. Tanemura, K. Kikuchi, T. Nagashima, T. Hasegawa, S. Ohara, and N. Sugimoto, "Experimental comparison of a Kerr nonlinearity figure of merit including the stimulated Brillouin scattering threshold for state-of-the-art nonlinear optical fibers," Opt. Lett. **30**, 1698–1700 (2005).
107. L. Zou, X. Bao, S. Afshar, and L. Chen, "Dependence of the Brillouin frequency shift on strain and temperature in a photonic crystal fiber," Opt. Lett. **29**, 1485–1487 (2004).
108. M. Ding, N. Hayashi, Y. Mizuno, and K. Nakamura, "Brillouin gain spectrum dependences on temperature and strain in erbium-doped optical fibers with different erbium concentrations," Appl. Phys. Lett. **102**, 191906 (2013).
109. Y. Mizuno, N. Hayashi, H. Tanaka, Y. Wada, and K. Nakamura, "Brillouin scattering in multi-core optical fibers for sensing applications," Sci. Rep. **5**, 11388 (2015).
110. Z. Zhao, M. A. Soto, M. Tang, and L. Thévenaz, "Distributed shape sensing using Brillouin scattering in multi-core fibers," Opt. Express **24**, 25211–25223 (2016).
111. Y. Mizuno and K. Nakamura, "Experimental study of Brillouin scattering in perfluorinated polymer optical fiber at telecommunication wavelength," Appl. Phys. Lett. **97**, 021103 (2010).
112. G. P. Agrawal, *Nonlinear Fiber Optics* (Academic, 1995).
113. Y. Mizuno and K. Nakamura, "Potential of Brillouin scattering in polymer optical fiber for strain-insensitive high-accuracy temperature sensing," Opt. Lett. **35**, 3985–3987 (2010).
114. N. Hayashi, Y. Mizuno, and K. Nakamura, "Brillouin gain spectrum dependence on large strain in perfluorinated graded-index polymer optical fiber," Opt. Express **20**, 21101–21106 (2012).
115. N. Hayashi, K. Minakawa, Y. Mizuno, and K. Nakamura, "Brillouin frequency shift hopping in polymer optical fiber," Appl. Phys. Lett. **105**, 091113 (2014).
116. Y. Mizuno, N. Matsutani, N. Hayashi, H. Lee, M. Tahara, H. Hosoda, and K. Nakamura, "Brillouin characterization of slimmed polymer optical fibers for strain sensing with extremely wide dynamic range," Opt. Express **26**, 28030–28037 (2018).
117. K. Minakawa, Y. Mizuno, and K. Nakamura, "Cross effect of strain and temperature on Brillouin frequency shift in polymer optical fibers," J. Lightwave Technol. **35**, 2481–2486 (2017).
118. A. Schreier, A. Wosniok, S. Liehr, and K. Krebber, "Humidity-induced Brillouin frequency shift in perfluorinated polymer optical fibers," Opt. Express **26**, 22307–22314 (2018).
119. Y. Mizuno, H. Lee, N. Hayashi, and K. Nakamura, "Hydrostatic pressure dependence of Brillouin frequency shift in polymer optical fibers," Appl. Phys. Express **11**, 012502 (2018).
120. Y. Dong, P. Xu, H. Zhang, Z. Lu, L. Chen, and X. Bao, "Characterization of evolution of mode coupling in a graded-index polymer optical fiber by using Brillouin optical time-domain analysis," Opt. Express **22**, 26510–26516 (2014).
121. A. Minardo, R. Bernini, and L. Zeni, "Distributed temperature sensing in polymer optical fiber by BOFDA," IEEE Photon. Technol. Lett. **26**, 387–390 (2014).
122. Y. Mizuno, Z. He, and K. Hotate, "One-end-access high-speed distributed strain measurement with 13-mm spatial resolution based on Brillouin optical correlation-domain reflectometry," IEEE Photon. Technol. Lett. **21**, 474–476 (2009).
123. Y. Mizuno, W. Zou, Z. He, and K. Hotate, "Operation of Brillouin optical correlation-domain reflectometry: theoretical analysis and experimental validation," J. Lightwave Technol. **28**, 3300–3306 (2010).
124. Y. Mizuno, N. Hayashi, H. Fukuda, K. Y. Song, and K. Nakamura, "Ultrahigh-speed distributed Brillouin reflectometry," Light Sci. Appl. **5**, e16184 (2016).
125. Y. Mizuno, H. Lee, and K. Nakamura, "Recent advances in Brillouin optical correlation-domain reflectometry," Appl. Sci. **8**, 1845 (2018).
126. N. Hayashi, Y. Mizuno, and K. Nakamura, "Distributed Brillouin sensing with centimeter-order spatial resolution in polymer optical fibers," J. Lightwave Technol. **32**, 3999–4003 (2014).
127. N. Hayashi, Y. Mizuno, and K. Nakamura, "Simplified Brillouin optical correlation-domain reflectometry using polymer optical fiber," IEEE Photon. J. **7**, 6800407 (2015).
128. Y. Mizuno, H. Lee, N. Hayashi, and K. Nakamura, "Noise suppression technique for distributed Brillouin sensing with polymer optical fibers," Opt. Lett. **44**, 2097–2100 (2019).
129. N. Hayashi, K. Minakawa, Y. Mizuno, and K. Nakamura, "Polarization scrambling in Brillouin optical correlation-domain reflectometry using polymer fibers," Appl. Phys. Express **8**, 062501 (2015).

130. H. Lee, N. Hayashi, Y. Mizuno, and K. Nakamura, "Slope-assisted Brillouin optical correlation-domain reflectometry using polymer optical fibers with high propagation loss," J. Lightwave Technol. **35**, 2306–2310 (2017).
131. A. Theodosiou and K. Kalli, "Recent trends and advances of fibre Bragg grating sensors in CYTOP polymer optical fibres," Opt. Fiber Technol. **54**, 102079 (2020).
132. G. Giaretta, W. White, M. Wegmuller, and T. Onishi, "High-speed (11 Gbit/s) data transmission using perfluorinated graded-index polymer optical fibers for short interconnects (<100 m)," IEEE Photon. Technol. Lett. **12**, 347–349 (2000).
133. C. Lethien, C. Loyez, J.-P. Vilcot, N. Rolland, and P. A. Rolland, "Exploit the bandwidth capacities of the perfluorinated graded index polymer optical fiber for multi-services distribution," Polymers **3**, 1006–1028 (2011).
134. A. Theodosiou, A. Lacraz, A. Stassis, C. Koutsides, M. Komodromos, and K. Kalli, "Plane-by-plane femtosecond laser inscription method for single-peak Bragg gratings in multimode CYTOP polymer optical fiber," J. Lightwave Technol. **35**, 5404–5410 (2017).
135. A. Theodosiou, M. Polis, A. Lacraz, M. Komodromos, A. Stassis, and K. Kalli, "Comparative study of multimode CYTOP graded index and single-mode silica fibre Bragg grating array for the mode shape capturing of a free-free metal beam," Proc. SPIE **9886**, 98860O (2016).
136. R. Min, B. Ortega, A. Leal-Junior, and C. Marques, "Fabrication and characterization of Bragg grating in CYTOP POF at 600-nm wavelength," IEEE Sens. Lett. **2**, 5000804 (2018).
137. M. Koerdt, S. Kibben, O. Bendig, S. Chandrashekhar, J. Hesselbach, C. Brauner, A. S. Herrmann, F. Vollertsen, and L. Kroll, "Fabrication and characterization of Bragg gratings in perfluorinated polymer optical fibers and their embedding in composites," Mechatronics **34**, 137–146 (2016).
138. R. Ishikawa, H. Lee, A. Lacraz, A. Theodosiou, K. Kalli, Y. Mizuno, and K. Nakamura, "Pressure dependence of fiber Bragg grating inscribed in perfluorinated polymer fiber," IEEE Photon. Technol. Lett. **29**, 2167–2170 (2017).
139. A. Theodosiou, M. Komodromos, and K. Kalli, "Carbon cantilever beam health inspection using a polymer fibre Bragg grating array," J. Lightwave Technol. **36**, 986–992 (2017).
140. A. Leal-Junior, A. Theodosiou, C. Marques, M. J. Pontes, K. Kalli, and A. Frizera, "Thermal treatments and compensation techniques for the improved response of FBG sensors in POFs," J. Lightwave Technol. **36**, 3611–3617 (2018).
141. A. Theodosiou, X. Hu, C. Caucheteur, and K. Kalli, "Bragg gratings and Fabry-Perot cavities in low-loss multimode CYTOP polymer fiber," IEEE Photon. Technol. Lett. **30**, 857–860 (2018).
142. Y. Mizuno, R. Ishikawa, H. Lee, A. Theodosiou, K. Kalli, and K. Nakamura, "Potential of discriminative sensing of strain and temperature using perfluorinated polymer FBG," IEEE Sens. J. **19**, 4458–4462 (2019).
143. Y. Mizuno, T. Ma, R. Ishikawa, H. Lee, A. Theodosiou, K. Kalli, and K. Nakamura, "Twist dependencies of strain and temperature sensitivities of perfluorinated graded-index polymer optical fiber Bragg gratings," Appl. Phys. Express **12**, 082007 (2019).
144. Z. Du, S. Deng, Y. Bei, Q. Huang, B. Wang, J. Huang, and G. Yu, "Adsorption behavior and mechanism of perfluorinated compounds on various adsorbents—a review," J. Hazard. Mater. **274**, 443–454 (2014).
145. G. Woyessa, A. Fasano, C. Markos, H. K. Rasmussen, and O. Bang, "Low loss polycarbonate polymer optical fiber for high temperature FBG humidity sensing," IEEE Photon. Technol. Lett. **29**, 575–578 (2017).
146. G. Woyessa, J. K. M. Pedersen, A. Fasano, K. Nielsen, C. Markos, H. R. Rasmussen, and O. Bang, "Zeonex-PMMA microstructured polymer optical FBGs for simultaneous humidity and temperature sensing," Opt. Lett. **42**, 1161–1164 (2017).
147. A. Pospori, C. Marques, G. Sagias, H. Lamela-Rivera, and D. J. Webb, "Novel thermal annealing methodology for permanent tuning polymer optical fiber Bragg gratings to longer wavelengths," Opt. Express **26**, 1411–1421 (2018).
148. M. Liang, X. Fang, G. Wu, G. Xue, and H. Li, "A fiber Bragg grating pressure sensor with temperature compensation based on diaphragm-cantilever structure," Optik **145**, 503–512 (2017).
149. K. Kalli, A. Theodosiou, and A. Lacraz, "Femtosecond laser inscribed Bragg grating arrays in long lengths of polymer optical fibres: a route to practical sensing with POF," Electron. Lett. **52**, 1626–1627 (2016).
150. A. G. Leal-Junior, A. Frizera, A. Theodosiou, C. Diaz, M. Jimenez, R. Min, M. J. Pontes, K. Kalli, and C. Marques, "Plane-by-plane written, low-loss polymer optical fiber Bragg grating arrays for multiparameter sensing in a smart walker," IEEE Sens. J. **19**, 9221–9228 (2019).
151. A. Leal-Junior, A. Theodosiou, C. Díaz, C. Marques, M. J. Pontes, K. Kalli, and A. Frizera, "Fiber Bragg gratings in CYTOP fibers embedded in a 3D-printed flexible support for assessment of human–robot interaction forces," Materials **11**, 2305 (2018).
152. A. G. Leal-Junior, A. Theodosiou, R. Min, J. Casa, C. Diaz, W. M. D. Santos, M. J. Pontes, A. A. G. Siqueira, C. Marques, K. Kalli, and A. Frizera, "Quasi-distributed torque and displacement sensing on a series elastic actuator's spring using FBG arrays inscribed in CYTOP fibers," IEEE Sens. J. **19**, 4054–4061 (2019).
153. D. Vilarinho, A. Theodosiou, M. F. Domingues, P. Andre, K. Kalli, P. Antunes, and C. Marques, "Foot plantar pressure monitoring with CYTOP Bragg gratings sensing system," in *11th International Joint Conference on Biomedical Engineering Systems and Technologies* (2018), pp. 25–29.
154. A. G. Leal-Junior, A. Theodosiou, A. Frizera, M. F. Domingues, C. Leitao, K. Kalli, P. Andre, P. Antunes, M. J. Pontes, and C. Marques, "Polymer optical fiber sensors approaches for insole instrumentation," in *Wearable Robotics: Challenges and Trends. WeRob 2018*, M. Carrozza, S. Micera, and J. Pons, eds., Biosystems & Biorobotics (2019), Vol. **22**, pp. 470–474.
155. D. Vilarinho, A. Theodosiou, C. Leitão, A. G. Leal-Junior, M. Domingues, K. Kalli, P. Andre, P. Antunes, and C. Marques, "POFBG-embedded cork insole for plantar pressure monitoring," Sensors **17**, 2924 (2017).
156. A. Abdelouhab, D. Dias, and N. Freitag, "Numerical analysis of the behaviour of mechanically stabilized earth walls reinforced with different types of strips," Geotex. Geomemb. **29**, 116–129 (2011).
157. H. K. Rasmussen, A. Fasano, P. Stajanca, G. Woyessa, M. Schukar, and O. Bang, "Mechanical characterization of drawn Zeonex, Topas, polycarbonate and PMMA microstructured polymer optical fibres," Opt. Mater. Express **8**, 3600–3614 (2018).
158. G. Woyessa, H. K. Rasmussen, and O. Bang, "Zeonex—a route towards low loss humidity insensitive single-mode step-index polymer optical fibre," Opt. Fiber Technol. **57**, 102231 (2020).
159. W. Yuan, A. Stefani, and O. Bang, "Tunable polymer fiber Bragg grating (FBG) inscription: fabrication of dual-FBG temperature compensated polymer optical fiber strain sensors," IEEE Photon. Technol. Lett. **24**, 401–403 (2012).
160. G. Rajan, M. Y. M. Noor, E. Ambikairajah, and G.-D. Peng, "Inscription of multiple Bragg gratings in a single-mode polymer optical fiber using a single phase mask and its analysis," IEEE Sens. J. **14**, 2384–2388 (2014).
161. I. P. Johnson, D. J. Webb, and K. Kalli, "Utilisation of thermal annealing to record multiplexed FBG sensors in multimode microstructured polymer optical fibre," Proc. SPIE **7753**, 77536T (2011).
162. C. Marques, G.-D. Peng, and D. J. Webb, "Highly sensitive liquid level monitoring system utilizing polymer fiber Bragg gratings," Opt. Express **23**, 6058–6072 (2015).
163. C. Marques, A. Pospori, D. Saez-Rodriguez, K. Nielsen, O. Bang, and D. J. Webb, "Aviation fuel gauging sensor utilizing multiple diaphragm sensors incorporating polymer optical fiber Bragg gratings," IEEE Sens. J. **16**, 6122–6129 (2016).